AIAA SciTech Forum
6-10 January 2020, Orlando, FL
AIAA Scitech 2020 Forum

10.2514/6.2020-0426

Impact of pressure and equivalence ratio on the plasma-assisted ignition of methane/air and ethylene/air mixtures

Nicholas E. Deak* Aurélie Bellemans†, and Fabrizio Bisetti‡
The University of Texas at Austin, Austin, TX, USA
Université Libre de Bruxelles, Brussels, Belgium

The ignition of CH_4 and C_2H_4 via nanosecond pulsed discharges (NSPD) is studied in a zero-dimensional isochoric and adiabatic reactor. An efficiency metric is defined by considering the time delay between the first pulse and ignition of the reactive mixture. Ignition efficiency is found to have a strong dependence on the pulse energy deposition rate, with a secondary dependence on peak pulse strength. Ambient pressure, temperature, and mixture composition are varied parametrically over ranges that reflect applications of practical interest, namely combustion in scramjets, and gas turbines for energy generation. Pressure is found to have a large effect on the maximum mean electron energy, controlling which excited species are generated, and the amount of energy required to ignite the mixture. Equivalence ratio is shown to have a non-monotonic effect on ignition efficiency, with ignition occurring fastest around moderately fuel-rich conditions. The roles of enhanced radical production and mixture heating in promoting faster ignition are separated by repeating ignition simulations with direct heating of the heavy species, thereby bypassing radical production by electron impact and deexcitation of heavy particles. It is found that C_2H_4 and CH_4 display opposite trends. While radical production promotes faster ignition of ethylene, direct heating of the methane/air mixture is advantageous. A possible explanation rests in the very high activation energy of the first hydrogen abstraction from methane, which benefits from heating more than it does from the presence of radicals. Our results point to the fact that the optimal energy deposition strategy may be fuel-dependent.

I. Nomenclature

E/N	=	Reduced electric field
p	=	Background gas pressure
Φ	=	Equivalence ratio
TTI	=	Time to ignition
u_g	=	Background gas internal energy
u_e	=	Electron energy
S_g	=	Electron energy source term
$Q_E(t)$	=	Pulse energy source term
ν_i^{el}	=	Collision frequency between electrons and species i
T_g	=	Background gas temperature
T_{g_e}	=	Electron temperature
$\delta\varepsilon_j$	=	Electron energy loss from inelastic collision reaction j
S_j^k	=	Production rate of species k via reaction j
$k_{f,j}$	=	Forward rate coefficient of reaction j
b_j	=	Coefficients for Janev rate coefficient fit of electron reaction j
X_i	=	Mole fraction of species i
f	=	Pulse frequency
P	=	Peak pulse power density

*Graduate Research Student, Dept. of Aerospace Engineering and Engineering Mechanics, 2617 Wichita Street, Austin, TX, USA.
†Postdoctoral Researcher, Département d'Aéro-Thermo-Mécanique, Ecole Polytechnique de Bruxelles, Université Libre de Bruxelles, Ixelles 1050, Belgium
‡Professor, Dept. of Aerospace Engineering and Engineering Mechanics, 2617 Wichita Street, Austin, TX, USA, AIAA Member

FWHM = Pulse full-width at half-maximum
E = Energy density per pulse

II. Introduction

Non-equilibrium plasma pulses have been shown to enhance combustion in a wide array of applications, ranging from vehicle propulsion [1], to energy production [2, 3], and from emissions reduction [4], to the synthesis of alternative fuels [5]. Non-equilibrium plasmas differ from thermal (equilibrium) plasmas, which have been used historically for ignition, in that they feature an electron temperature that exceeds the background gas temperature [6]. A voltage between two electrodes is applied, which creates an electric field that imparts energy primarily to the electrons. The energized electrons then transfer energy to the other particles through elastic and inelastic collisions, which include collisions resulting in rotational, vibrational, and electronic excitation, dissociation, and ionization. The primary mode of energy transfer depends on the mean energy attained by the electrons during the pulse, which is itself a function of the reduced electric field E/N, and the thermodynamic conditions of the mixture [7].

Non-equilibrium plasmas have been shown to enhance combustion through three mechanisms [8]. The first is the thermal effect, whereby the plasma pulses raise the temperature of the mixture through ohmic heating, which accelerates combustion reactions. The second is through the production of key radicals that would not otherwise be present, as well as the breaking up of large fuel fragments through collisions with electrons and other excited species. The third effect is the change non-equilibrium plasmas can induce in transport processes by electrohydrodynamic forces.

In recent years, nanosecond pulsed discharges (NSPD) have emerged as a promising technique in enhancing ignition and combustion, due to their ability to generate high-energy electrons. NSPD feature a short plasma discharge over tens of nanoseconds (O(10-100) ns), during which a high voltage is applied (1-100 kV), creating a high electric field (100-1000 Td) [9]. The high electric field creates highly energetic electrons, which collide with heavy species, such as N_2, O_2, and hydrocarbons. Collisions involving high-energy electrons are conducive to creating excited species, ions, and radicals through impact dissociation. Following the application of the pulse, electronically excited species such as N_2^* and O_2^* are rapidly quenched through collisions with other heavy species, on a time scale of a few tens of nanoseconds. These collisions often lead to further dissociation of O_2 and N_2, creating O and N radicals which quickly thermalize, in a process known as fast heating [10]. Production of radicals in this manner is far more effective when compared with traditional ignition methods, where radicals are primarily created through thermal dissociation, which requires higher temperatures [11]. Additional heating occurs through the relaxation of vibrationally excited species, primarily N_2, on a time scale of 1-10 μs, in a process known as slow heating [12]. Thus, the use of NSPD can be an effective way of both raising the gas temperature and creating key radicals that enhance combustion.

NSPD have been applied to a wide array of combustion technologies of practical interest in recent years, and have been shown to help in areas such as ignition, flame stability, and emission control. In this work, two application areas are chosen to focus the study. The first is combustion for ramjet and scramjet propulsion. Flow conditions in supersonic applications are such that the characteristic flow residence times τ_{flow} are shorter than typical ignition times τ_{ign}, or the time required for complete combustion τ_c. On the other hand, rapid heat release can cause thermal choking, leading to engine unstart [13]. It is clear then that a good deal of control over the ignition and combustion processes is required. To investigate this application, ethylene/air mixtures at 0.5 atm, 800 K, and equivalence ratios varying from 0.33-3.0 are considered, and the time to ignition (TTI) is measured to gauge performance.

Another application of importance is lean and ultra-lean combustion, as fuel efficiency and emissions reduction become areas of greater focus. The use of non-equilibrium plasmas show benefits in areas such as power generation through lean gas turbines, flameless combustion, and combustion of alternative fuels, through reduction of CO_2 and NO_x [14], enabling combustion at lower temperatures [15], and extension of lean blowout/flammability limits [16]. The conditions in these applications make combustion unreliable, with low temperatures, high pressures ($p > 10$ atm), and ultra lean mixtures ($\phi < 0.5$). Among the primary challenges in lean combustion are ignition and flame stabilization. To explore this application area, the ignition efficiency of lean methane/air mixtures ($0.4 < \phi < 0.7$) at pressures ranging from 0.5-30 atm are investigated in V.

In this study, we first explore the ideal pulse settings to achieve ignition of a given mixture most efficiently. We then consider the extent to which non-equilibrium plasma pulses help ignite a mixture over traditional heating methods, and how this changes for different fuels. Next, we examine the ignition efficiency of ethylene-air mixtures change as we move from ultra-lean to fuel rich regimes. Finally, we explore the impact of increasing pressure on the ignition efficiency of lean methane-air mixtures.

This paper is organized as follows. III discusses the system of equations to be solved, and the methods used to solve

them. IV introduces in greater detail the kinetic mechanism used to carry out the simulations in this study. Results are presented in V. Finally, VI presents conclusions and explores future research opportunities.

III. Governing Equations and Methods

Simulations of methane/air and ethylene air ignition via NSPD have been conducted in an isochoric and adiabatic zero-dimensional reactor. We adopt a two-temperature plasma model, where heavy species share a single temperature, while electrons have their own. This model has been shown to be accurate for weakly ionized plasmas at a range of pressures, which is appropriate for the applications in question. The applications under consideration involve initial pressures ranging from $p_0 \approx 0.5$ atm (supersonic combustion), to $p_0 \geq 30$ atm (lean combustors for power generation).

In the standard heating case, it is assumed that the entirety of the energy delivered goes to the much less massive electrons, rather than heavier ions in the gas mixture. This results in a population of excited electrons that transfer their energy to the heavier species, primarily through inelastic collisions.

In this work, non-equilibrium plasma is generated through high-voltage pulses occurring on a nanosecond time scale (O(10-100 ns)). In the zero-dimensional reactor model, transport is neglected. The simulation requires the integration of the evolution of the bulk gas internal energy, mean electron energy, and species number density, which are given as

$$\frac{\partial u_g}{\partial t} = S_g \tag{1}$$

$$\frac{\partial u_e}{\partial t} = S_e \tag{2}$$

$$\frac{\partial n_k}{\partial t} = \sum_{j=1}^{R} S_j^k, \tag{3}$$

where u_g is the bulk gas internal energy (J/kg-m^3), u_e is the mean electron energy, and n_k is the number density of species k. There are a total of N species and R reactions in the kinetic mechanism. The mean electron energy is calculated as $n\bar{\epsilon}$, with $\bar{\epsilon} = (3/2)k_B T_e$. The species source terms S_j^k are obtained from the CHEMKIN library, and summed over R reactions for each species. These reactions include both plasma reactions (electron - neutral collisions, and excited species quenching), as well as traditional combustion reactions. A detailed description of the plasma/combustion kinetics model is provided later in IV.

The electron energy source term S_e consists of several components,

$$S_e = Q_E(t) + 3k_B \left(\sum_{i=1}^{N} \nu_i^{el} \frac{m_e}{m_i} \right) n_e (T_e - T_g) - \sum_{j=1}^{R} \delta\varepsilon_j S_j^e. \tag{4}$$

In the equation above, the first term, $Q_E(t)$, is the input energy from the discharge. Each pulse follows a Gaussian profile, which is defined by the pulse full width at half maximum (FWHM), peak power density P, and the pulse frequency f. A total of N_p pulses are delivered to the mixture. The next term represents the energy transfer due to elastic collisions between electrons and all other species, and is negative when the electron temperature exceeds the gas temperature, generally during and shortly after each pulse. The summation is over N heavy species, where ν_i^{el} is the collision frequency between electrons and species i, and $m_{e,i}$ represents the electron and species i masses, respectively. The final term represents energy transfer between electrons and all other particles due to inelastic collisions, including vibrational/electronic excitation, as well as collisions resulting in dissociation, and ionization, with each collision j contributing to a change of energy $\delta\epsilon_j$.

The source term in the internal energy equation is $S_g = -S_e + Q_E(t)$. Thus, energy from each pulse increases the mean electron energy, which decreases shortly after (on a nanosecond time scale) due to electron collisions with heavier species. According to the model, heavy species don't receive any energy directly from the pulse, rather from collisions with excited electrons. These collisions serve to both directly heat up the gas, and create excited species and radicals, both of which promote ignition.

In V, the role of radical production and heating are separated by modifying the model equations. The baseline case outlined above is compared with a"direct heating" strategy, where the pulse energy $Q_E(t)$ is given directly to the mixture

of heavy species. In this case, the equations outlined above remain the same, except for S_e, which is instead defined as:

$$S_e = 3k_B \left(\sum_{i=1}^{N} \nu_i^{el} \frac{m_e}{m_i} \right) n_e (T_e - T_g) - \sum_{j=1}^{R} \delta\varepsilon_j S_j^e . \tag{5}$$

Solution of the system of equations outlined above is achieved using the CVODE solver part of the SUNDIALS suite of ODE solvers [17]. An adaptive time stepping technique is used, with shorter time steps taken during pulses to ensure plasma chemistry is adequately resolved, and longer time steps in between pulses. In order to ensure that the variables of interest are computed accurately, a relative tolerance $\epsilon_r = 10^{-13}$ is used, along with absolute tolerances of $\epsilon_T = 10^{-8}$ and $\epsilon_C = 10^{-30}$ for the temperature and concentrations, respectively. Thermodynamic properties for all plasma and combustion processes are evaluated by a two-temperature extension of the CHEMKIN library [18].

IV. Kinetic Mechanism

We adopt the plasma/combustion mechanism proposed by Eckert et al. [19]. The mechanism has been modified to include elastic electron collisions, and improved rate coefficient fits for elastic and inelastic electron collisions. The mechanism includes a plasma reaction model, consisting of 379 reactions describing electron collisions with 10 different species as well as excited species quenching reactions, and a combustion model consisting of 163 species and 1085 reactions. The plasma model accounts for electron collisions resulting in the vibrational and electronic excitation, dissociation, and ionization of various species, as well as electron recombination. The combustion model describes the oxidation of CH_4 and C_2H_4 fuels.

When electrons gain energy through a NSD pulse, they reach a maximum mean energy dependent primarily on the pulse strength, and the pressure of the gas mixture. The excited electrons then lose energy to the background gas mixture heavy species through elastic and inelastic collisions. In the model under consideration, the inelastic electron collisions are comprised of those that result in vibrational and electronic excitation, impact dissociation, and ionization of various heavy species. In total, the model considers electron collisions with 8 ground state species, and 2 ions: N_2, O_2, O, H_2, C_2H_4, C_2H_2, CH_4, C_3H_8, N_2^+, and O_2^+.

The rate coefficients of inelastic electron collisions are assumed to depend on the energy of the electron, which is related to the reduced electric field E/N. The rate coefficient data for electron collisions at various reduced electric field values has been obtained from BOLSIG+ [20], which solves the Boltzmann equation at various E/N values to obtain rate and transport coefficient data. The rate coefficient data as a function of the mean electron energy has been fit using the functional form:

$$k_{f,j} = A_j \exp\left(\sum_{n=1}^{9} b_{n,j} (\ln T_e)^{n-1} \right). \tag{6}$$

This reaction rate coefficient, along with an excitation parameter that describes the amount of energy lost by the electron (expressed in eV) fully describe the electron process. Cross-section data, which is used as input to BOLSIG+ for calculating rate coefficients, are obtained from the Morgan database available on LXCat [21]. Electron collision reactions are summarized in VII.A. Comparisons of data from BOLSIG+ against the Janev fit (as well a FIT1 fit, another type often used for modeling electron collision rate coefficients) are provided in Fig. 1 for the vibrational excitation of N_2 ($E + N_2 \rightarrow E + N_2(v1)$).

Although vibrational excitation reactions are considered for all relevant species, N_2 is the only species for which the relative population of each vibrational state is described (v1-8). Likewise, we only model various electronically excited states of $N_2(A^3\Sigma, B^3\Pi, W^3\Delta, B^3\Sigma, a^1\Sigma, a^1\Pi, w^1\Delta, C^3\Pi, E^3\Sigma, ap^1\Sigma)$, $O_2(a^1\Delta, b^1\Sigma)$, and O(1D, 1S). All other collisions that result in electronic excitation are neglected. Elastic collisions and collisions resulting in heavy species dissociation are considered for all relevant species in the plasma model. Finally, collisions resulting in ionization of O_2 and N_2 are included, resulting in 3 charged species(E, N_2^+, and O_2^+).

As mentioned previously, electron collisions with 8 ground state species are considered. Thus, electron collisions involving radicals, excited species, and other electrons are omitted, as are superelastic collisions. In the two-fluid model, it is known that for low values of E/N (as seen, for instance, shortly after a NSD pulse), the electron temperature may drop below the background gas temperature, as inelastic collisions with low energy thresholds continue to transfer energy from electrons to the heavy species. This non-physical behavior is due to the omission of superelastic collisions, which would otherwise transfer energy from energized heavy species to the electrons [20]. Although it has no appreciable

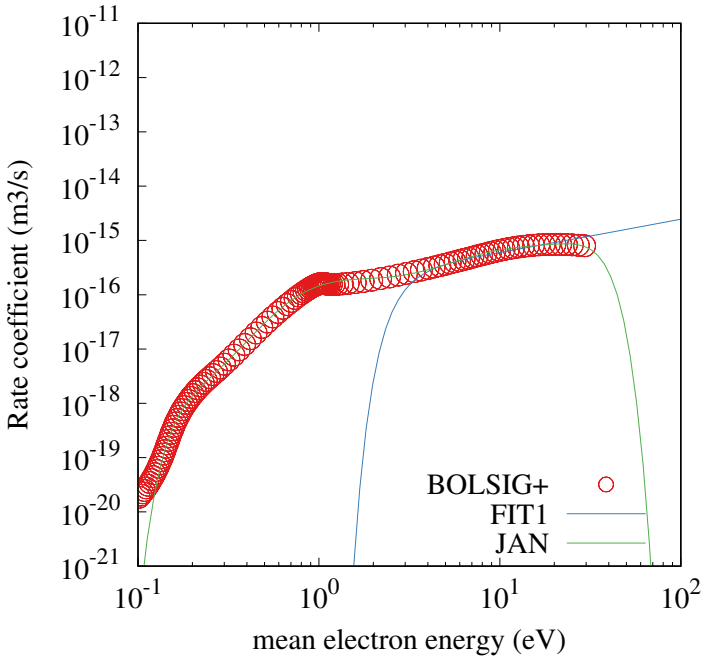

Fig. 1 Comparison of BOLSIG+ data against Janev and FIT1 fits for the vibrational excitation of N_2, for a range of mean electron energies

effect on the final results, this issue has been addressed by applying a threshold function to the energy source term S_ε which tends to zero when the difference between the electron and gas temperatures is small.

V. Results and Discussion

This section discusses a range of conclusions drawn from the 0D ignition study. First, an overview of the mixture ignition process is provided in section V.A. Next, the effect of pulsing parameters on ignition efficiency is examined in section V.B. The effect of pressure on ignition efficiency for different gas heating models are compared for both methane and ethylene in section V.C. Finally The effect of different equivalence ratios on time to ignition (TTI) is considered incorporated into the analysis in section V.D.

A. Ignition Overview

The ignition of fuel/air mixtures via NSPD is simulated with a two-temperature isochoric and adiabatic reactor for a wide range of conditions. The study considers methane and ethylene fuels, various stoichiometries, and initial pressures p_0 from 0.5 to 30 atm. The discharge parameters are varied across a wide range of values, and are chosen to ensure ignition occurs within a practically relevant amount of time (O(10 - 100) μs. Discharge frequencies between 5 and 500 kHz, FWHM between 15 and 120 ns, and single pulse energy densities (E) between 15 and 15,000 J / cm^3 are explored. A wide range of energy densities is explored due to the wide range of pressures, with low pressure cases (p_0 = 0.5 atm) corresponding with E O)(10 - 100) J / cm^3, and high pressure cases (p_0 = 30 atm) corresponding with E O)(1000 - 10,000) J / cm^3. The reactor is initialized with pressure $p = p_0$, temperature $T = T_e = T_0$(= 800 K for all cases), and a mixture of fuel and air with equivalence ratio Φ.

The temporal evolution of a reactive mixture during a NSPD, characteristic of all ignition events considered in this study, is presented in Fig. 2. Values of energy density per pulse employed in the study were chosen to be comparable to those in experimental studies of NSPD. Lefkowitz et al. [22] report using 0.8-3.2 mJ per pulse in a discharge channel volume of ~17 mm^3 to ignite a mixture of methane and air at 1 atm and 850 K. The plasma formed during the discharges occupies a thin cylindrical channel bridging between the electrodes. The channel's volume is approximately 0.018 cm^{-3}, resulting in a single-pulse energy density O(100 mJ/cm^3), which is comparable to those used in the study

It is apparent that the electron reaches peak mean energies $\varepsilon \approx 6.5$ eV during the discharge, followed by rapid cooling

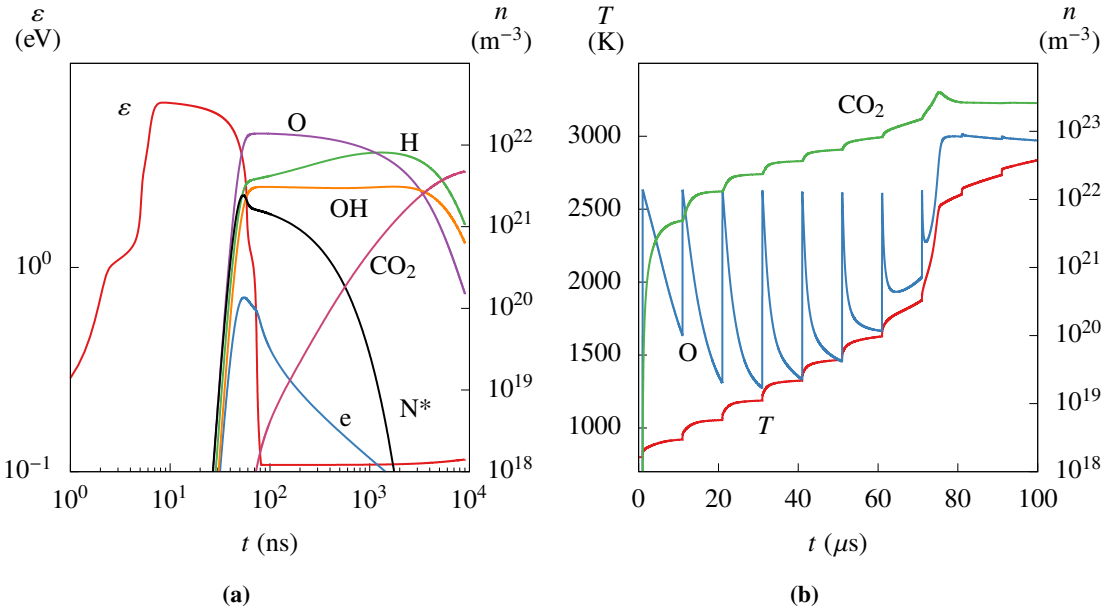

Fig. 2 Time evolution of the mean electron energy ε, number density of select species and gas temperature during ignition of a 0.5 atm stoichiometric methane/air mixture for (a) a single pulse and (b) multiple pulses (E = 31.9 mJ cm^{-3}, FWHM = 15 ns, and f = 100 kHz)

as electrons lose energy through collisions with neutral particles. Energetic electrons form excited state particles, mostly through inelastic collisions with O_2 and N_2 and the quenching reactions that follow excitation (e.g. $N_2^* + O_2 \rightarrow N_2 + 2O$) result in the formation of radicals as the electronically excited particles thermalize. This process is known as *ultra-fast heating* [23], marked by a modest increase in T. Following ultra-fast heating, the temperature continues to increase, albeit more slowly, in a process known as *slow heating* [12]. This is largely due to VT relaxation of vibrationally excited N_2.

Figure 2 also shows the temporal evolution of electronically excited nitrogen N_2^*, various combustion radicals, namely O, H, and OH, as well as important combustion products (CO and CO_2). O and H radicals are created through the fast heating process described above, as well as through dissociation of O_2 and fuel species via electron impact. These radicals are important in breaking down the fuel and fuel fragments, and help promote the production of CO and CO_2. It is seen that the populations of combustion radicals reach a peak following each pulse, while their subsequent consumption coincides with an increase in the populations of CO and CO_2, which accumulate with each pulse (along with gas temperature).

Figure 3 provides further insight into the processes occurring during each pulse, and shows the fraction of electron energy lost Ω through various collision processes. It is apparent that leading up to the peak of the pulse ($\sim$ 50 ns) when the electric field is strongest, neutral particle electronic excitation and dissociation represent a majority of the electron energy losses. This is consistent with the fact that electronic excitation and dissociation of neutral particles (primarily O_2 and N_2) have relatively high electron energy thresholds ($\sim 6 - 12$ eV). In contrast, as the electric field strength drops following the pulse peak, vibrational excitation becomes the primary pathway for electron energy loss, consistent with the lower energy thresholds for vibrational excitation ($\sim 0.1 - 3$ eV).

Following the accumulation of CO_2 and modest increase in temperature following each pulse, the concentration of carbon dioxide increases abruptly. This rapid acceleration, driven by conventional exothermic reactions, is consistent with an *ignition event*. Thus, the instant in time when the rate of change of the number density of CO_2 peaks is taken to represent the time of ignition t^*. Then, the *time to ignition* (TTI) is defined as TTI = $t^* - t_1$, where t_1 is the timing of the peak discharge power during the first pulse. Thus, TTI represents the interval between the first pulse and ignition. This is shown schematically in Fig. 4.

B. Ignition Strategy

The impact of pulsing parameters on TTI was investigated using stoichiometric methane/air and ethylene/air mixtures at 0.5 atm, and 800 K, characteristic of the conditions seen in the supersonic combustion applications discussed in

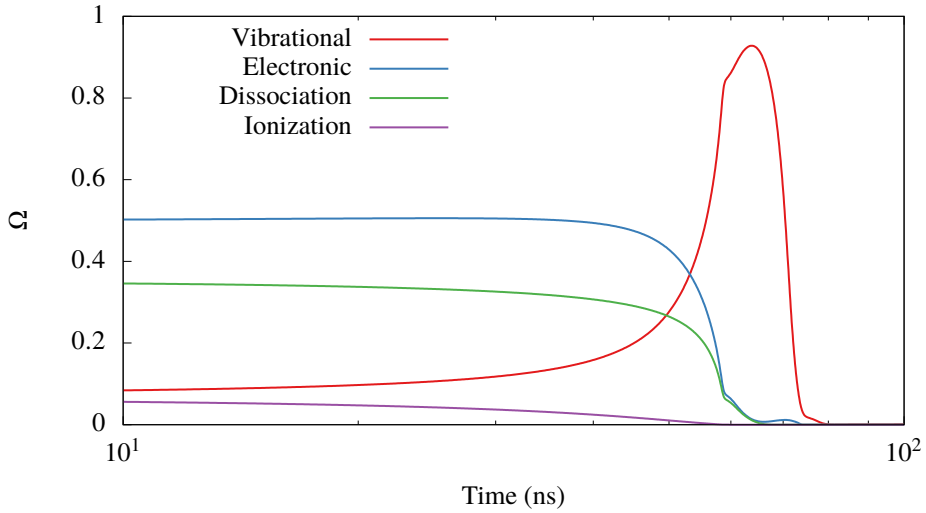

Fig. 3 Fraction of electron energy lost Ω through vibrational excitation, electronic excitation, dissociation, and ionization of neutral particles.

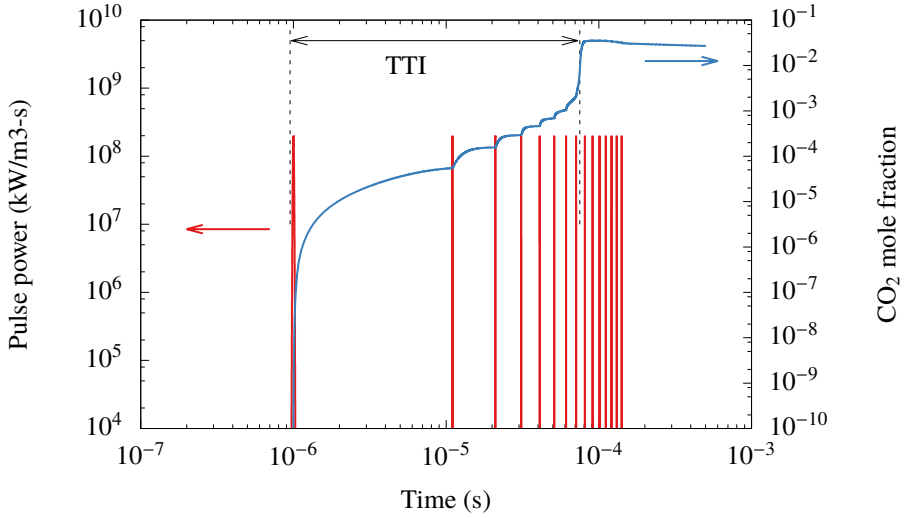

Fig. 4 Measurement of TTI using the pulse power, and CO_2 concentration

section II. Pulse frequency f has been varied from 5-500 kHz, peak power density P is varied from 500 - 480,000 kW/cm^3, and pulse FWHM is varied from 15-120 ns. Given the Gaussian pulse profile used in the study, P and FWHM can be used to calculate the energy density per pulse as $E = P\sqrt{2\pi}\sigma$, with $\sigma = \text{FWHM}/(2\sqrt{2\ln 2})$. TTI for each case can then be plotted against the energy deposition rate W, calculated as $E * f$. Results are presented in Fig. 5 for methane (a) and ethylene (b).

Several results can be drawn immediately from the data. First both fuels display a power law dependence of TTI on W, with faster ignition obtained for larger energy deposition rates. Since the energy deposition rate is the product the pulse frequency and the energy density per pulse, one can conclude that these two factors alone do not play a primary role in determining TTI, and that weaker, more frequent pulses are roughly equivalent to stronger, infrequent pulses. Second, for a given W, ethylene ignites more readily than does methane. Finally, it appears that there is a secondary effect of pulse FWHM on TTI. For a given W, a larger FWHM corresponds with a lower peak pulse power P, while the opposite is true for shorter FWHM values.

This is seen more clearly in Fig. 6a, which illustrates the impact of pulse FWHM on TTI for both fuels, for an energy

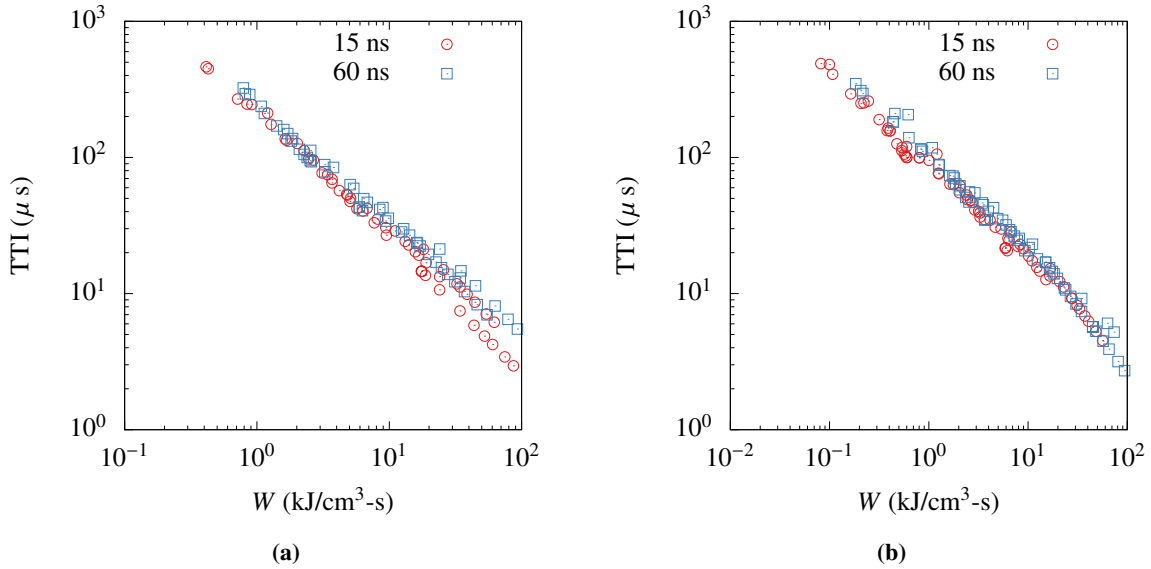

Fig. 5 TTI as a function of energy deposition rate for 15 and 60 ns FWHM pulses at various f and P for methane/air mixtures (a) and ethylene/air mixtures (b).

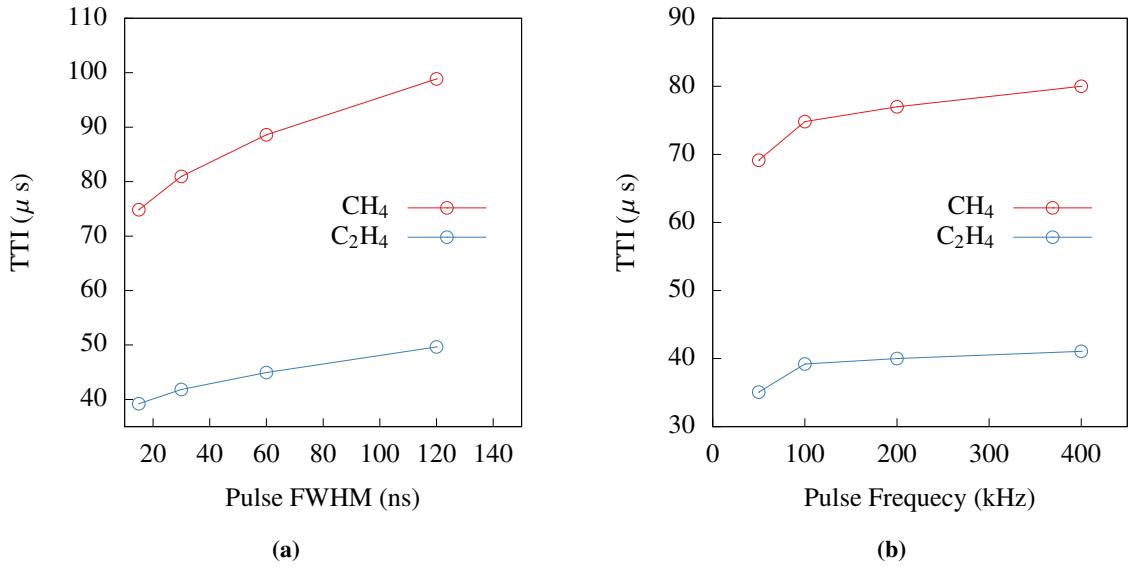

Fig. 6 TTI as a function of (a) pulse FWHM for constant W, f, and E and (b) pulse frequency for a constant W and FWHM.

deposition rate of 3.2 kW/cm^3 , a pulse frequency of 100 kHz, and a single-pulse energy density of 32 mJ/cm^3. In order to keep E constant, the peak pulse power P is increased in proportion with decreases in FWHM. As FWHM decreases and P increases, the mixture ignites more efficiently, as a shorter TTI is achieved with the same power deposition. In addition, the dependence of TTI on f is shown in Fig. 6b, with a fixed energy deposition rate of 3.2 kW/cm^3, and a pulse FWHM of 15 ns. In order to hold W constant, the single-pulse energy density E is increased proportionally with decreases in f. It is apparent that all else held constant, lower pulse frequencies, and thus higher single-pulse energy densities, lead to a more efficient ignition.

To summarize, TTI is primarily governed by the energy deposition rate. Secondary dependencies of TTI on pulse FWHM (holding W, f, and E constant), and pulse frequency (holding W and FWHM constant) are also observed. It is

found that for a given energy deposition rate, higher peak pulse powers and single-pulse energy densities are preferable for obtaining a faster ignition.

C. Pressure Dependence

The impact of pressure on TTI is examined for both methane/air and ethylene/air mixtures. In an effort to differentiate the kinetic effects of non-equilibrium plasma pulses from the ohmic heating effects, two different mixture heating models are considered, as defined in section III. In the standard plasma heating case, pulse energy goes towards energizing the electrons in the mixture. In this case, the gas is heated both directly, through ohmic heating, as well as kinetic changes to the mixture induced by the excited electrons. In contrast, the direct heating case represents a purely thermal ignition, where energy is given directly to the gas itself. In this case, highly energized electrons are not present, and excited plasma species (electronically excited and ionized O_2 and N_2) are not generated. The direct heating case is then representative of more standard methods of ignition, which use thermal plasmas to heat a mixture and achieve ignition.

The two heating models are tested on stoichiometric methane/air mixture ethylene/air mixtures. A series of methane/air and ethylene/air simulations are run for $0.5 < p_0 < 30$ atm. The pulse settings used were FWHM = 15 ns and $f = 100$ kHz. Starting from $p_0 = 0.5$ atm and $W = 3.4$ kJ cm^{-3} s^{-1}, the pressure is varied and W is adjusted in order to keep the mean energy deposition rate per unit mass constant. In practice, this means that as p_0 increases, W increases by the same factor. Results are presented in 7.

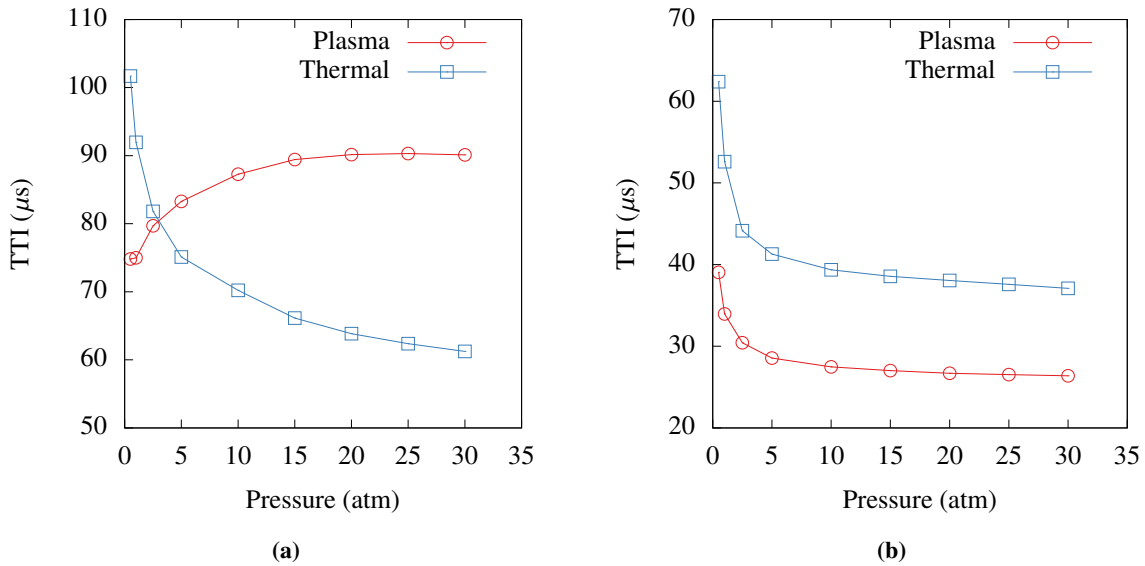

Fig. 7 TTI as a function of pressure for both the plasma heating and direct (thermal) heating models, shown for methane/air mixtures (a), and ethylene/air mixtures (b).

Looking at Fig. 7, several conclusions can be drawn. First, the results highlight a clear distinction between the behavior of ethylene and methane when subject to NSPD. Looking at Fig. 7b, it is apparent that ethylene ignites more rapidly when the same amount of energy is supplied via non-equilibrium plasma pulses across all pressures tested. A very different trend is observed looking at Fig. 7a, which shows TTI for methane at various pressures for both heating models. At low pressures ($p \leq 2.5$ atm), plasma heating marginally outperforms direct gas heating, however this trend reverses as pressure is increased, and indicate that at higher pressures, direct heating is more efficient at igniting mixtures. It is also interesting to note that the ignition of methane/air via NSPD behaves differently compared with all other cases, as TTI increases with increasing pressure. The reason for this is discussed briefly below.

The trend observed for ethylene is similar to previously observed trends for the ignition of H_2-O_2 mixtures [24]. Although not discussed in this paper, the reason for improved performance of NSPD over direct heating for ethylene/air ignition but not methane ignition can be summarized as follows. The primary benefit NSPD imparts on the ignition process is the generation of substantial populations of combustion radicals (O, H, and OH) at low temperatures where they would otherwise not be present. These radicals are crucial in the breakdown of the fuel, as well as fuel radicals

(i.e. CH_3, C_2H_3, HCO) and other intermediate species such as formaldehyde (CH_2O) that are formed during the fuel breakdown process, ultimately forming CO and CO_2.

In the case of methane/air ignition, oxidation occurs through a series of intermediates, $CH_4 \rightarrow CH_3 \rightarrow CH_2O \rightarrow HCO \rightarrow CO$, where the first three steps require the presence of combustion radicals. There is a bottleneck in the breakdown of formaldehyde into HCO at higher pressures, which occurs inefficiently until later in the ignition process when classic high temperature combustion pathways take over, limiting the effectiveness of the radicals. This is due to the well known chain termination step $H + O_2 \leftrightarrow HO_2$, which limits the availability of H for breaking down formaldehyde. In the case of ethylene/air ignition, the sequence of steps in the oxidation process is much more complex, and there exist several bypass pathways that allow for the formation of CO through pathways that don't involve formaldehyde. These pathways remain active at both low and high pressure, allowing for efficient oxidation of ethylene via NSPD for all pressures considered.

D. Ignition and Equivalence Ratio

Ignition efficiency and flame stability are of great importance when it comes to the combustion of both methane/air and ethylene/air mixtures. Ethylene is a proxy for fuels used in supersonic combustion; conditions in supersonic combustors are often highly turbulent and chaotic, and mixture properties such as local equivalence ratio can vary greatly from location to location. Methane is used as a fuel in gas turbines for power generation, where lean conditions and high pressures can create problems for flame stability.

In order to explore the effect of non-equilibrium plasma on mixtures of varying equivalence ratio Φ, a series of ethylene/air simulations have been run for $p_0 = 0.5$ atm and $T_0 = 800$ K. Pulse settings have been kept the same for each simulation, with pulse FWHM = 10 ns, $f = 200$ kHz, $P = 500$ kW/cm^3. Enough pulses have been used to ensure that for each simulation, ignition occurs prior to the final pulse. Results for both plasma heating and direct heating strategies are presented in Fig. 8:

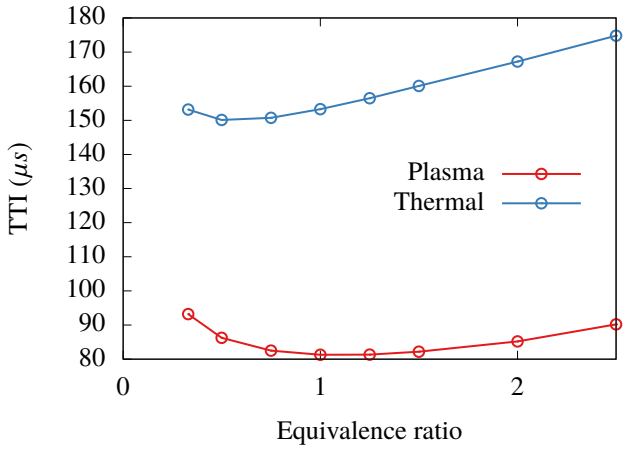

Fig. 8 Effect of equivalence ratio on ignition of ethylene-air mixtures for both plasma heating and direct (thermal) heating models ($p_0 = 0.5$ atm, $T_0 = 800$ K, FWHM = 10 ns, $f = 200$ kHz, and $P = 500$ kW/cm^3).

As seen in section V.C, for ethylene/air mixtures, the plasma heating is a more efficient strategy than direct heating across pressures. This trend holds true across equivalence ratios as well. It is also interesting to note that peak ignition efficiency occurs at different points for each strategy, with ignition occurring earliest at stoichiometric and slightly fuel rich conditions for the plasma heating strategy, and at lean conditions in the case of direct heating. As expected, as conditions become very lean or very rich, ignition efficiency drops.

The analysis presented in section V.C is expanded to include equivalence ratio effects. As in section V.C, a series of methane/air and ethylene/air simulations are run for $0.5 < p_0 < 30$ atm, with $0.5 < \Phi < 1, .0$ for methane, and $0.5 < \Phi < 1.5$ for ethylene. The pulse settings used were FWHM = 15 ns and $f = 100$ kHz. Starting from $p_0 = 0.5$ atm and $W = 3.4$ kJ cm^{-3} s^{-1}, the pressure is varied and W is adjusted in order to keep the mean energy deposition rate per unit mass constant. Results are presented for methane/air and ethylene air in Fig. 9.

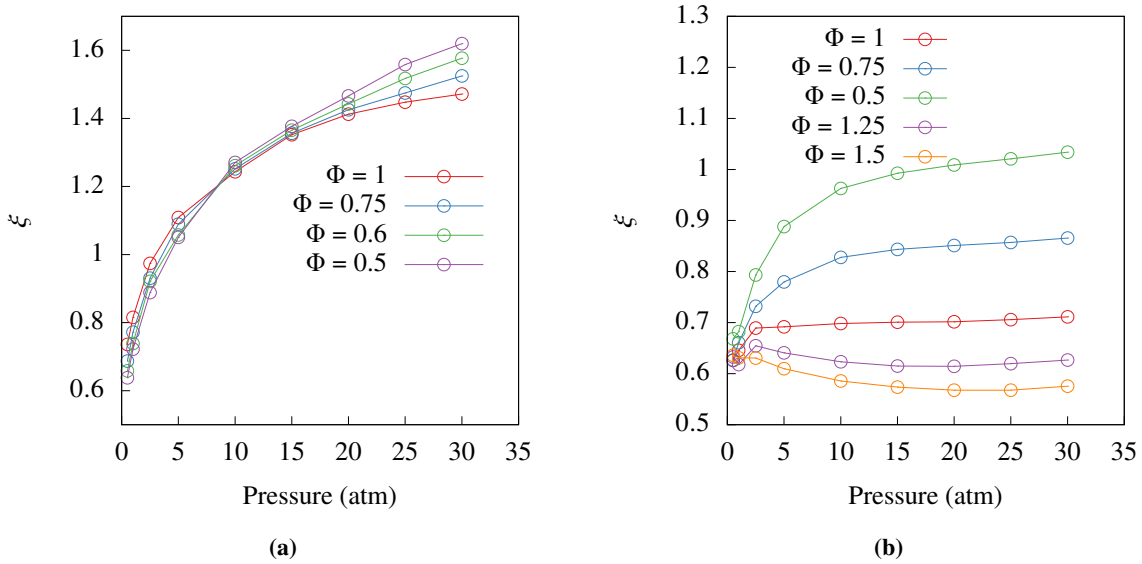

Fig. 9 Ratio of time to ignition $\xi = \mathrm{TTI}/\tau_T$ as a function of p_0, keeping the energy per unit mass constant for (a) methane/air and (b) ethylene/air.

Several conclusions can be drawn from the results. First, it is apparent that in comparison with ethylene, methane ignition is fairly insensitive to equivalence ratio, as the trends in pressure observed at stoichiometric conditions persist for leaner mixtures. At higher pressures ($p_0 > 20$ atm), there is a minor equivalence ratio effect, with leaner mixtures taking a relatively longer amount of time to ignite (compared with the thermal ignition time τ_T).

Ethylene ignition, in contrast shows a greater dependence on equivalence ratio. It is apparent that the trends shown in Fig. 8 for 0.5 persist at higher pressures as well, namely that for a given pressure, plasma ignition performs best under slightly fuel-rich conditions, while thermal ignition performs well under slightly lean conditions. The equivalence ratio and pressure trends interact, leading to an appreciable decrease in ignition efficiency for lean fuels under high pressure conditions. In fact, for the leanest mixtures tested in this study ($\Phi = 0.5$), thermal ignition outperforms plasma ignition ($\xi > 1$) for pressures exceeding 20 atm.

An interesting departure in these trends is observed for fuel-rich ethylene/air mixtures. In contrast to all other cases discussed, plasma ignition efficiency actually improves relative to thermal ignition with increasing pressure. This would indicate that the trends observed in Fig. 8 become exaggerated as pressure increases.

VI. Conclusion

In this study, the ignition of methane-air and ethylene-air mixtures using non-equilibrium NSD plasma pulses is studied using a 0D two-temperature model. A robust kinetic mechanism, which couples a plasma model to a to a hydrocarbon fuel combustion model, is used in the investigation. Quantities of interest, such as pulse settings, pressure, and equivalence ratio are varied parametrically to determine the ideal ignition strategy under a wide range of conditions. It is found that ignition efficiency is closely tied to the pulse energy deposition rate, with a secondary dependence on other pulse parameters, such as the peak pulse power, and single-pulse energy deposition. Specifically, shorter, stronger pulses are more effective at igniting mixtures than longer, weaker pulses.

In order to gauge the benefit of using non-equilibrium plasma in the mixture ignition process, two different heating models are considered - a standard plasma heating model where pulse energy is given entirely to the electrons in the mixture, and a direct heating model where pulse energy is given directly to the gas. It is found for ethylene, the direct gas heating model under-performs for a wide range of pressures and equivalence ratios compared with plasma heating, whereas the opposite is found to be true for methane-air mixtures at initial pressures greater than 1 atm.

Equivalence ratio effects for methane/air and ethylene/air are also considered. Results indicate that when using the standard plasma heating model, ignition occurs faster near stoichiometric to slightly fuel-rich conditions for ethylene. For the direct gas heating model, however, ignition is favored under slightly fuel-lean conditions. These trends seem to

be enhanced with increasing pressure. Methane/air ignition, meanwhile, shows only a minor dependence on equivalence ratio.

It is important to keep in mind that all results discussed above are obtained from a 0D model, with no modeling of transport of any kind. In order to further validate the conclusions drawn from this study and draw more definitive conclusions, future works will need to investigate the above trends using multi-dimensional, unsteady ignition of reactive mixtures in the presence of turbulence and mixture stratification.

VII. Acknowledgments

Nicholas Deak and Fabrizio Bisetti are sponsored by the National Science Foundation through NSF grant number 1903775, under program manager Harsha Chelliah. Aurélie Bellemans is supported by a fellowship through the Belgian American Educational Foundation and the F.R.S - FNRS (Belgian Fund for Research).

References

[1] Takita, K., Abe, N., Masuya, G., and Ju, Y., "Ignition enhancement by addition of NO and NO2 from a N2/O2 plasma torch in a supersonic flow," *Proceedings of the Combustion Institute*, Vol. 31, No. 2, 2007, pp. 2489–2496.

[2] Pilla, G., Galley, D., Lacoste, D. A., Lacas, F., Veynante, D., and Laux, C. O., "Stabilization of a turbulent premixed flame using a nanosecond repetitively pulsed plasma," *IEEE Transactions on Plasma Science*, Vol. 34, No. 6, 2006, pp. 2471–2477.

[3] Choi, W.-S., Neumeier, Y., and Jagoda, J., "Stabilization of a combustion process near lean blow off by an electric discharge," *42nd AIAA Aerospace Sciences Meeting and Exhibit*, 2004, p. 982.

[4] Khacef, A., Cormier, J. M., and Pouvesle, J. M., "NOx remediation in oxygen-rich exhaust gas using atmospheric pressure non-thermal plasma generated by a pulsed nanosecond dielectric barrier discharge," *Journal of Physics D: Applied Physics*, Vol. 35, No. 13, 2002, p. 1491.

[5] Paulmier, T., and Fulcheri, L., "Use of non-thermal plasma for hydrocarbon reforming," *Chemical engineering journal*, Vol. 106, No. 1, 2005, pp. 59–71.

[6] Ju, Y., and Sun, W., "Plasma assisted combustion: Dynamics and chemistry," *Progress in Energy and Combustion Science*, Vol. 48, 2015, pp. 21–83.

[7] Starikovskiy, A., and Aleksandrov, N., "Plasma-assisted ignition and combustion," *Progress in Energy and Combustion Science*, Vol. 39, No. 1, 2013, pp. 61–110.

[8] Ju, Y., Lefkowitz, J. K., Reuter, C. B., Won, S. H., Yang, X., Yang, S., Sun, W., Jiang, Z., and Chen, Q., "Plasma assisted low temperature combustion," *Plasma Chemistry and Plasma Processing*, Vol. 36, No. 1, 2016, pp. 85–105.

[9] Starikovskaia, S. M., "Plasma assisted ignition and combustion," *Journal of Physics D: Applied Physics*, Vol. 39, No. 16, 2006, p. R265.

[10] Popov, N., "Fast gas heating in a nitrogen–oxygen discharge plasma: I. Kinetic mechanism," *Journal of Physics D: Applied Physics*, Vol. 44, No. 28, 2011, p. 285201.

[11] Breden, D., and Raja, L., "Simulations of nanosecond pulsed plasmas in supersonic flows for combustion applications," *AIAA journal*, Vol. 50, No. 3, 2012, pp. 647–658.

[12] Lanier, S., Shkurenkov, I., Adamovich, I. V., and Lempert, W. R., "Two-stage energy thermalization mechanism in nanosecond pulse discharges in air and hydrogen–air mixtures," *Plasma Sources Science and Technology*, Vol. 24, No. 2, 2015, p. 025005.

[13] Billig, F. S., "Research on supersonic combustion," *Journal of Propulsion and Power*, Vol. 9, No. 4, 1993, pp. 499–514.

[14] Kim, H., Takashima, K., Katsura, S., and Mizuno, A., "Low-temperature NOx reduction processes using combined systems of pulsed corona discharge and catalysts," *Journal of Physics D: Applied Physics*, Vol. 34, No. 4, 2001, p. 604.

[15] Sun, W., Won, S. H., and Ju, Y., "In situ plasma activated low temperature chemistry and the S-curve transition in DME/oxygen/helium mixture," *Combustion and Flame*, Vol. 161, No. 8, 2014, pp. 2054–2063.

[16] Bak, M. S., Do, H., Mungal, M. G., and Cappelli, M. A., "Plasma-assisted stabilization of laminar premixed methane/air flames around the lean flammability limit," *Combustion and Flame*, Vol. 159, No. 10, 2012, pp. 3128–3137.

[17] Hindmarsh, A. C., Brown, P. N., Grant, K. E., Lee, S. L., Serban, R., Shumaker, D. E., and Woodward, C. S., "SUNDIALS: Suite of nonlinear and differential/algebraic equation solvers," *ACM Transactions on Mathematical Software*, Vol. 31, No. 3, 2005, pp. 363–396.

[18] Kee, R. J., Rupley, F. M., and Miller, J. A., "Chemkin-II: A Fortran chemical kinetics package for the analysis of gas-phase chemical kinetics," Tech. rep., Sandia National Labs., Livermore, CA (USA), 1989.

[19] Eckert, Z. S., "Energy Transfer in Non-Equilibrium Reacting Gas Flows: Applications in Plasma Assisted Combustion and Chemical Gas Lasers," Ph.D. thesis, The Ohio State University, 2018.

[20] Hagelaar, G., and Pitchford, L., "Solving the Boltzmann equation to obtain electron transport coefficients and rate coefficients for fluid models," *Plasma Sources Science and Technology*, Vol. 14, No. 4, 2005, p. 722.

[21] Pancheshnyi, S., Biagi, S., Bordage, M., Hagelaar, G., Morgan, W., Phelps, A., and Pitchford, L., "The LXCat project: Electron scattering cross sections and swarm parameters for low temperature plasma modeling," *Chemical Physics*, Vol. 398, 2012, pp. 148–153.

[22] Lefkowitz, J. K., Guo, P., Ombrello, T., Won, S. H., Stevens, C. A., Hoke, J. L., Schauer, F., and Ju, Y., "Schlieren imaging and pulsed detonation engine testing of ignition by a nanosecond repetitively pulsed discharge," *Combustion and Flame*, Vol. 162, No. 6, 2015, pp. 2496–2507.

[23] Shkurenkov, I., and Adamovich, I. V., "Energy balance in nanosecond pulse discharges in nitrogen and air," *Plasma Sources Science and Technology*, Vol. 25, No. 1, 2016, p. 015021.

[24] Tholin, F., Lacoste, D. A., and Bourdon, A., "Influence of fast-heating processes and O atom production by a nanosecond spark discharge on the ignition of a lean H2–air premixed flame," *Combustion and Flame*, Vol. 161, No. 5, 2014, pp. 1235–1246.

Appendix

A. Electron Collisions

No.	Reaction	A	Exci.	b_1	b_2	b_3	b_4	b_5	b_6	b_7	b_8	b_9
	Elastic collisions											
R1	$N_2 + E \rightarrow N_2 + E$	2.72e-07	–	-1.07e+0	7.11e-1	-4.02e-1	-5.13e-3	2.32e-1	-7.62e-2	-3.9e-2	2.48e-2	-3.51e-3
R2	$O_2 + E \rightarrow O_2 + E$	2.30e-07	–	-1.58e+0	3.55e-1	-1.52e-1	2.70e-1	3.54e-2	-9.13e-2	4.78e-3	1.14e-2	-2.21e-3
R3	$O + E \rightarrow O + E$	4.36e-07	–	-2.51e+0	6.87e-1	1.06e-1	2.48e-1	-9.60e-1	1.09e+0	-5.38e-1	1.22e-1	-1.04e-2
R4	$C_2H_4 + E \rightarrow C_2H_4 + E$	2.90e-07	–	-7.62e-1	4.11e-1	-1.95e-1	1.70e-1	1.61e-2	-4.76e-2	3.31e-3	4.42e-3	-7.87e-4
R5	$CH_4 + E \rightarrow CH_4 + E$	2.076e-07	–	-2.04e+0	1.73e+0	-7.65e-2	-2.13e-1	1.98e-2	1.01e-2	-3.03e-4	-1.57e-4	-5.83e-5
	Vibrational excitation											
R6	$N_2 + E \rightarrow N_2(v1) + E$	8.499e-10	0.29	-1.5e+0	2.93e-1	-5.43e-1	9.13e-1	-4.23e-2	-2.4e-1	3.75e-2	2.25e-2	-5.21e-3
R7	$N_2 + E \rightarrow N_2(v1) + E$	4.425e-09	0.29	-2.22e-2	2.38e+0	-4.99e+0	1.58e+0	2.01e+0	-1.11e+0	-2.95e-1	2.71e-1	-4.24e-2
R8	$N_2 + E \rightarrow N_2(v2) + E$	2.574e-09	0.59	5.37e-2	3.19e+0	-7.21e+0	2.51e+0	2.95e+0	-1.71e+0	-4.06e-1	3.97e-1	-6.28e-2
R9	$N_2 + E \rightarrow N_2(v3) + E$	1.764e-09	0.88	1.89e-1	4.02e+0	-9.76e+0	3.69e+0	3.93e+0	-2.4e+0	-4.93e-1	5.25e-1	-8.4e-2
R10	$N_2 + E \rightarrow N_2(v4) + E$	1.102e-09	1.17	-2.63e-1	-3.88e-1	-4.8e+0	2.92e+1	-5.17e+1	4.27e+1	-1.85e+1	4.04e+0	-3.54e-1
R11	$N_2 + E \rightarrow N_2(v5) + E$	8.681e-10	1.47	-3.71e-1	4.21e-2	-5.67e+0	2.95e+1	-5.02e+1	4.08e+1	-1.75e+1	3.79e+0	-3.31e-1
R12	$N_2 + E \rightarrow N_2(v6) + E$	6.763e-10	1.76	-5.13e-1	-9.7e-1	-7.61e+0	4.98e+1	-8.87e+1	7.37e+1	-3.19e+1	7.01e+0	-6.15e-1
R13	$N_2 + E \rightarrow N_2(v7) + E$	3.441e-10	2.06	-7.18e-1	-1.5e+0	-8.48e+0	6.22e+1	-1.13e+2	9.51e+1	-4.16e+1	9.18e+0	-8.09e-1
R14	$N_2 + E \rightarrow N_2(v8) + E$	1.568e-10	2.35	-1.01e+0	1.25e+0	-1.13e+1	4.69e+1	-7.48e+1	5.9e+1	-2.48e+1	5.33e+0	-4.61e-1
R15	$O_2 + E \rightarrow O_2 + E$	1.632e-09	0.19	-2.41e+0	1.24e-1	-1.68e+1	8.91e+1	-1.51e+2	1.23e+2	-5.29e+1	1.16e+1	-1.01e+0
R16	$O_2 + E \rightarrow O_2 + E$	4.031e-10	0.19	-5.44e-1	-7.16e-1	-8.36e-2	-4.7e-2	-1.43e-1	3.24e-2	1.53e-2	5.2e-4	-1.32e-3
R17	$O_2 + E \rightarrow O_2 + E$	7.343e-10	0.38	-2.68e+0	3.4e+0	-1.52e+1	5.19e+1	-7.75e+1	5.94e+1	-2.46e+1	5.24e+0	-4.5e-1
R18	$O_2 + E \rightarrow O_2 + E$	1.262e-10	0.38	-2.52e-1	-6.57e-1	-4.23e-1	1.95e-1	-9.47e-2	-2.91e-2	5.17e-3	1.37e-2	-3.46e-3
R19	$O_2 + E \rightarrow O_2 + E$	4.202e-10	0.57	-2.14e+0	1.07e+0	5.58e-1	2.38e-1	-3.32e-1	-3.86e-2	1.69e-2	2.07e-2	-5.29e-3
R20	$O_2 + E \rightarrow O_2 + E$	2.359e-10	0.75	-2.47e+0	1.77e+0	2.52e-1	1.07e-1	-2.69e-1	-2.43e-3	1.87e-3	1.89e-2	-4.45e-3
R21	$C_2H_4 + E \rightarrow C_2H_4 + E$	7.174e-09	0.11	-1.07e-1	2.53e-1	-2.67e-1	7.71e-2	1.1e-1	-7.98e-2	-1.11e-2	1.68e-2	-2.88e-3
R22	$C_2H_4 + E \rightarrow C_2H_4 + E$	2.097e-09	0.36	-1.08e-1	2.31e-1	-2.13e-1	1.01e-1	1.48e-2	-3.66e-2	-4.84e-3	9.24e-3	-1.67e-3
R23	$CH_4 + E \rightarrow CH_4 + E$	1.228e-08	0.16	-1.64e+0	7.25e-1	5.42e-1	-1.19e-1	-1.72e-1	2.78e-2	1.66e-2	-1.01e-3	-7.65e-4
R24	$CH_4 + E \rightarrow CH_4 + E$	9.827e-09	0.36	-1.79e+0	1.26e+0	3.72e-1	-1.44e-1	-1.75e-1	3.11e-2	1.1e-2	3.29e-3	-1.58e-3
	Electronic excitation											
R25	$N_2 + E \rightarrow N_2(A^3\Sigma) + E$	1.818e-10	6.17	-4.65e+0	3.38e+0	-1.77e+1	6.7e+1	-1.04e+2	8.12e+1	-3.42e+1	7.37e+0	-6.39e-1
R26	$N_2 + E \rightarrow N_2(A^3\Sigma) + E$	7.774e-10	7.00	-4.89e+0	3.54e+0	-1.85e+1	7e+1	-1.08e+2	8.48e+1	-3.57e+1	7.69e+0	-6.67e-1
R27	$N_2 + E \rightarrow N_2(B^3\Pi) + E$	2.060e-09	7.35	-4.43e+0	3.49e+0	-1.86e+1	7.05e+1	-1.09e+2	8.51e+1	-3.58e+1	7.69e+0	-6.66e-1

R28	$N_2 + E \rightarrow N_2(W^3\Delta) + E$	2.335e-09	7.36	-5.19e+0	4.43e+0	-1.78e+1	6.04e+1	-8.99e+1	6.91e+1	-2.88e+1	6.19e+0	-5.35e-1
R29	$N_2 + E \rightarrow N_2(A^3\Sigma) + E$	7.773e-10	7.80	-5.36e+0	4.61e+0	-1.88e+1	6.39e+1	-9.52e+1	7.32e+1	-3.05e+1	6.54e+0	-5.65e-1
R30	$N_2 + E \rightarrow N_2(B^3\Sigma) + E$	7.107e-10	8.16	-5.22e+0	2.96e+0	-2.06e+1	8.64e+1	-1.38e+2	1.09e+2	-4.63e+1	1e+1	-8.73e-1
R31	$N_2 + E \rightarrow N_2(a^1\Sigma) + E$	5.626e-10	8.40	-5.27e+0	3.01e+0	-2.1e+1	8.82e+1	-1.41e+2	1.12e+2	-4.73e+1	1.02e+1	-8.91e-1
R32	$N_2 + E \rightarrow N_2(a^1\Pi) + E$	3.183e-09	8.55	-6.25e+0	3.98e+0	-2.03e+1	7.69e+1	-1.19e+2	9.31e+1	-3.92e+1	8.46e+0	-7.34e-1
R33	$N_2 + E \rightarrow N_2(w^1\Delta) + E$	5.859e-10	8.89	-5.21e+0	4.88e+0	-2.01e+1	6.84e+1	-1.02e+2	7.8e+1	-3.24e+1	6.94e+0	-5.98e-1
R34	$N_2 + E \rightarrow N_2(C^3\Pi) + E$	5.515e-09	11.03	-7.11e+0	6.34e+0	-2.55e+1	8.64e+1	-1.28e+2	9.81e+1	-4.08e+1	8.72e+0	-7.52e-1
R35	$N_2 + E \rightarrow N_2(E^3\Sigma) + E$	5.739e-11	11.88	-9.04e+0	8.26e+0	-2.31e+1	6.33e+1	-8.59e+1	6.32e+1	-2.58e+1	5.47e+0	-4.7e-1
R36	$N_2 + E \rightarrow N_2(ap^1\Sigma) + E$	4.070e-10	12.25	-9.18e+0	8.67e+0	-2.41e+1	6.59e+1	-8.91e+1	6.52e+1	-2.65e+1	5.59e+0	-4.79e-1
R37	$O_2 + E \rightarrow O_2(a^1\Delta) + E$	9.563e-10	0.98	-2.3e+0	3.36e+0	-1.7e+0	-8.97e-1	1.35e+0	-1.71e-2	-4.96e-1	2.12e-1	-2.67e-2
R38	$O_2 + E \rightarrow O_2(b^1\Sigma) + E$	2.312e-10	1.63	-2.7e+0	5.29e+0	-4.14e+0	-2.44e-1	1.86e+0	-3.95e-1	-3.69e-1	1.79e-1	-2.23e-2
R39	$O + E \rightarrow O(1D) + E$	3.364e-09	1.97	-2.43e+0	3.22e+0	-1.04e+1	3.23e+1	-4.71e+1	3.56e+1	-1.47e+1	3.1e+0	-2.66e-1
R40	$O + E \rightarrow O(1S) + E$	3.422e-10	4.19	-3.27e+0	3.86e+0	-1.41e+1	4.36e+1	-6.28e+1	4.73e+1	-1.94e+1	4.11e+0	-3.51e-1
	Impact dissociation											
R41	$N_2 + E \rightarrow N + N + E$	3.418e-08	13.00	-1.18e+1	8.72e+0	-2.82e+1	8.63e+1	-1.23e+2	9.26e+1	-3.82e+1	8.16e+0	-7.03e-1
R42	$O_2 + E \rightarrow O + O + E$	5.892e-10	4.50	-2.4e+0	2.64e+0	-1.59e+1	6.1e+1	-9.45e+1	7.37e+1	-3.09e+1	6.62e+0	-5.72e-1
R43	$O_2 + E \rightarrow O + O(1D) + E$	1.805e-09	6.00	-3.11e+0	3.57e+0	-1.58e+1	5.44e+1	-8.12e+1	6.23e+1	-2.58e+1	5.51e+0	-4.74e-1
R44	$O_2 + E \rightarrow O(1D) + O(1D) + E$	3.084e-08	8.40	-5.58e+0	4.34e+0	-1.84e+1	6.33e+1	-9.48e+1	7.3e+1	-3.04e+1	6.49e+0	-5.6e-1
R45	$O_2 + E \rightarrow O + O(1S) + E$	9.434e-10	9.97	-9.27e+0	4.57e+0	-2.33e+1	8.87e+1	-1.37e+2	1.08e+2	-4.55e+1	9.82e+0	-8.53e-1
R46	$C_2H_4 + E \rightarrow C_2H_3 + H + E$	3.730e-09	3.80	-2.31e+0	3.13e+0	-1.46e+1	5.02e+1	-7.52e+1	5.77e+1	-2.39e+1	5.09e+0	-4.37e-1
R47	$C_2H_4 + E \rightarrow C_2H_3 + H + E$	9.059e-08	5.00	-5.59e+0	4.32e+0	-1.48e+1	4.6e+1	-6.64e+1	5.04e+1	-2.08e+1	4.43e+0	-3.81e-1
R48	$C_2H_4 + E \rightarrow C_2H_3 + H + E$	2.348e-08	7.00	-6.06e+0	4.36e+0	-1.76e+1	6.01e+1	-8.99e+1	6.94e+1	-2.9e+1	6.21e+0	-5.37e-1
R49	$CH_4 + E \rightarrow CH_3 + H + E$	1.384e-08	10.00	-7.01e+0	4.16e+0	-2.26e+1	8.67e+1	-1.34e+2	1.05e+2	-4.44e+1	9.58e+0	-8.31e-1
R50	$CH_4 + E \rightarrow CH_3 + H + E$	1.369e-08	11.00	-7.9e+0	5.68e+0	-2.37e+1	8.15e+1	-1.22e+2	9.37e+1	-3.91e+1	8.37e+0	-7.24e-1
R51	$CH_4 + E \rightarrow CH_3 + H + E$	1.354e-08	12.00	-8.88e+0	7.3e+0	-2.48e+1	7.63e+1	-1.09e+2	8.22e+1	-3.38e+1	7.2e+0	-6.19e-1
	Impact ionization											
R52	$N_2 + E \rightarrow N_2^+ + E + E$	3.345e-08	15.60	-1.52e+1	1.22e+1	-3.44e+1	9.54e+1	-1.3e+2	9.56e+1	-3.89e+1	8.23e+0	-7.06e-1
R53	$O_2 + E \rightarrow O_2^+ + E + E$	3.925e-08	12.06	-1.15e+1	4.46e+0	-2.95e+1	1.25e+2	-2e+2	1.59e+2	-6.77e+1	1.47e+1	-1.28e+0